Sensible Heat Flux in Near-Neutral Conditions over the Sea

L. MAHRT

NorthWest Research Associates (Seattle Division), Corvallis, Oregon

DEAN VICKERS

CEOAS, Oregon State University, Corvallis, Oregon

EDGAR L ANDREAS

NorthWest Research Associates (Seattle Division), Lebanon, New Hampshire

DJAMAL KHELIF

Department of Mechanical and Aerospace Engineering, University of California, Irvine, Irvine, California

(Manuscript received 12 October 2011, in final form 10 February 2012)

ABSTRACT

The variation of the sea surface sensible heat flux is investigated using data from the Gulf of Tehuantepec Experiment (GOTEX) and from eight additional aircraft datasets representing a variety of surface conditions. This analysis focuses on near-neutral conditions because these conditions are common over the sea and are normally neglected, partly because of uncertain reliability of measurements of the small air–sea temperature difference. For all of the datasets, upward heat flux is observed for slightly stable conditions. The frequency of this ''countergradient'' heat flux increases with increasing wind speed and is possibly related to sea spray or microscale variations of surface temperature on the wave scale. Upward area-averaged sensible heat flux for slightly stable conditions can also be generated by mesoscale heterogeneity of the sea surface temperature (SST). Significant measurement errors cannot be ruled out.

The countergradient heat flux for weakly stable conditions is least systematic for weaker winds, even though it occurs with weak winds in all of the datasets. In an effort to reduce offset errors and different SST processing and calibration procedures among field programs, the authors adjusted the SST in each field program to minimize the countergradient flux for weak winds. With or without this adjustment for the combined dataset, the extent of the upward heat flux for weakly stable conditions increases with increasing wind speed.

1. Introduction

Direct estimates of the transfer coefficients for sensible heat flux and other scalars are particularly problematic for near-neutral conditions because relatively small errors in the air–sea temperature difference may strongly contaminate the estimated transfer coefficient. Therefore, such conditions are generally excluded from analysis. Although the sensible heat flux is small in near-neutral conditions (typically less than 10 W m^{-2}), such conditions may cover a large fraction of the earth's open oceans and thus contribute significantly to the global heat budget. Small deviations from neutral stratification toward unstable stratification can significantly enhance the transport of sensible heat and other scalars even beyond that predicted by similarity theory (Smedman et al. 2007a,b) because of augmentation of the flux in a transition of eddy structure from neutral to slightly unstable conditions.

Mahrt and Khelif (2010, and references therein) find that, for weakly stable, spatially averaged air–sea temperature difference and even modest horizontal variation of the sea surface temperature (SST), the area-averaged sensible heat flux may be upward. Significant upward

Corresponding author address: Larry Mahrt, 2171 NW Kari Pl., Corvallis, OR 97330.
E-mail: mahrt@nwra.com

DOI: 10.1175/JPO-D-11-0186.1

sensible heat flux occurs in small subareas with unstable stratification, which dominate the area-averaged sensible heat flux. In the larger subareas of weakly stable air–sea temperature difference, the downward sensible heat flux is quite small. However, the larger subareas of weakly stable stratification dominate the spatially averaged air–sea temperature difference such that the spatially averaged sensible heat flux is ''countergradient.'' These countergradient cases occur with weak winds as also found in Kalogiros and Wang (2011). Significant SST variations occur on a wide variety of horizontal scales (e.g., Zappa et al. 2004; Marmorino et al. 2004; Walsh 1998; Hagan et al. 1997), all of which alter the relationship between the area-averaged sensible heat flux and the area-averaged air–sea temperature difference.

The evolution of SST gradients is the net result of complex interactions among a number of processes, including the important impact of diurnal variation of radiative forcing and mixing in the upper ocean, particularly under weak-wind conditions (e.g., Katsaros and Soloviev 2004; Katsaros et al. 2005; Soloviev and Lukas 2006). Variations of SST often involve interactions with the surface stress and mixing within the upper ocean, which can vary substantially with weak winds (Grachev et al. 2003).

The relationship between the sensible heat flux and the SST is also influenced by microscale variations on the wave scale. Sea spray droplets form with the same temperature as the sea surface but cool rapidly (on the order of a second) to a temperature below the local air temperature because they essentially act as highly curved, saline wet bulbs (Andreas 1995). When the bigger droplets fall back into the sea (the reentrant droplets), they leave this sensible heat behind. As a result, spray droplets almost always contribute an upward flux of sensible heat while undergoing little evaporation. Andreas and Emanuel (2001) explain the full thermodynamics of this process. In high winds (10–12 m s^{-1} and above), under stable stratification, this upward spray-mediated sensible heat flux may be larger in magnitude than the downward sensible heat flux that results from the positive air–sea difference of potential temperature. The measured flux thus appears to be countergradient (Andreas 2011).

Previous studies of the sea surface sensible heat flux generally exclude countergradient heat fluxes by 1) eliminating them as apparent observational errors (e.g., Zeng et al. 1998); 2) imposing conditions on the minimum magnitude of the air–sea temperature difference such as 1 K or more, as in numerous studies; or 3) adjusting the surface radiation temperature to reduce the frequency of countergradient cases without consideration of wind speed (e.g., Vickers and Mahrt 2006). In contrast, this study examines the systematic behavior of the upward sensible heat flux in weakly stable conditions by analyzing aircraft data from the Gulf of Tehuantepec Experiment (GOTEX) without restrictions on the data. In addition, we briefly analyze data from eight additional aircraft field programs. No data are discarded based on heterogeneity and nonstationarity or other suspected causes of deviations from similarity theory.

2. Data

a. Field programs

The GOTEX aircraft data (Raga and Abarca 2007) analyzed here consist of nine flights with sufficient data for analysis of fluxes. We use only data from GOTEX flight levels between 30 and 40 m. Normally, the flux and wind vary only slowly within this height range such that the exact height of the aircraft is not important. Although the GOTEX data do not include very stable cases with semicollapsed turbulence, we cannot rule out underestimation of downward sensible heat flux due to flux divergence between the aircraft level and the surface. We do not attempt to correct for flux divergence through tenuous downward extrapolation from flights levels above 40 m.

We found a significant dependence of the wind and momentum fluxes on the flight direction with respect to the mean wind direction. This dependence on the flight direction was substantially reduced after the GOTEX data were reprocessed at the National Center for Atmospheric Research (Boulder, Colorado) in 2010.

A given variable ϕ, such as potential temperature or one of the velocity components, is initially partitioned as

$$\phi' = \phi - \overline{\phi}, \tag{1}$$

where the overbar averages over a flight segment of length $\tau = 1$ km to separate the turbulence from the larger-scale flow. The fluxes are computed from the product of perturbations quantities from Eq. (1),

$$\overline{w'\phi'}, \tag{2}$$

where w' is the perturbation in vertical velocity.

To reduce sampling problems, turbulence covariances are normally averaged over a longer distance τ_F, sometimes referred to as the flux-averaging length,

$$F = [\overline{w'\phi'}] = [w'\phi'], \tag{3}$$

where the brackets correspond to averaging over the longer averaging length τ_F and the turbulent quantities are defined as in Eq. (1). Because all averages are simple unweighted averages, the overbar becomes redundant

TABLE 1. Field program, general location, number of 4-km segments, range of flight levels, $\theta_{sfc} - \theta(z)$ corresponding to vanishing sensible heat flux (K), and references with more description of the data.

Site	Location	Segments	Level	$\theta_{sfc} - \theta(z)$	Reference
GOTEX	Central America	859	30–40	0.0	Raga and Abarca (2007)
SHOWEX-97	North Carolina	508	10–15	−1.0	Sun et al. (2001)
SHOWEX-99	North Carolina	970	10–15	−1.0	Sun et al. (2001)
CARMA4	Monterey, California	650	30–40	−0.7	
Monterey-08	Monterey, California	654	30–40	−1.2	Mahrt and Khelif (2010)
TOGA COARE	Tropical	938	30–40	−0.5	Sun et al. (1996)
MABLEB	Monterey, California	45	30–40	−0.4	
POST	Monterey, California	189	30–40	−0.5	
RED	Oahu, Hawaii	373	30–40	−0.5	Anderson et al. (2004)
CBLAST WEAK	Massachusetts	740	10–15	−2.2	Edson et al. (2007)

after averaging over τ_F, provided that τ_F is an integer multiple of τ. We examine the sensitivity to these choices of the averaging lengths in section 2c.

Eight additional aircraft datasets (Table 1) are analyzed to provide a larger range of conditions. For the multiexperiment analysis only, fluxes are computed for relatively short 4-km segments of the flight track to reduce the impact of surface heterogeneity ($\tau = \tau_F = 4$ km). Fluxes from the small 4-km segments suffer large flux sampling errors. Consequently, the fluxes are composited over intervals of a governing parameter such as the air–sea temperature difference (bin averaging). Such averages are not true ensemble averages in that variations within the interval are not due to random variations alone. Instead, some of the variation results from variation of physical parameters among 4-km segments within a given interval. The 4-km segments are thus not different realizations of exactly the same background physics. Averages of the fluxes within a given interval might be an underestimation of an ensemble average because fluxes may reverse sign between segments within a given interval because of differences in physical forcing.

For several of the datasets, the wind field, the momentum flux, or both exhibited systematic dependence on aircraft heading with respect to the mean wind direction. Such a dependence contributes to additional scatter in the between-variable relationships. Some of the analyses in this study are framed in terms of different wind speed categories. Because the height of the flight track varied from about 10 to 40 m among the datasets, winds were tentatively adjusted to a common 10-m level using similarity theory. However, this adjustment had no significant influence on the composited results for the different wind speed classes. Therefore, we avoid using similarity theory for the wind speed classification and simply composite according to the flight-level wind speed.

b. SST

Measurements of SST from aircraft are generally problematic (Burns et al. 2000; Donlon et al. 2002). Documentation of radiometer calibration and maintenance procedures for previous field programs are often incomplete or nonexistent. These errors are normally considered to be greater than errors in the measured air temperature. For Cloud-Aerosol Research in the Marine Atmosphere 4 (CARMA4), Marine Atmospheric Boundary Layer Energy Budget (MABLEB), Physics of Stratocumulus Top (POST), and Rough Evaporation Duct (RED), the Center for Interdisciplinary Remotely-Piloted Aircraft Studies (CIRPAS) Twin Otter measured the SST with a Heimann KT19.85 infrared pyrometer. No corrections to the SST were made for the upward reflection of downward longwave radiation. This omission is equivalent to assuming a longwave emissivity of unity for the sea surface while the actual emissivity is generally 0.98–0.99. This assumption is also used to convert the measured upward longwave radiation to the SST.

SHOWEX consisted of three 1-month field programs: November 1997, March 1999, and November 1999. The Everest 4000.4GXL infrared temperature sensor used on the LongEZ to measure sea surface temperature was corrected using temperature-dependent calibrations, which tended to drift slightly with time. As a result, additional daily adjustments were made by comparing the aircraft measurements with buoy measurements of the SST. The SST measurement varied erratically during the March 1999 field program, and those data are not used here.

c. Offset and wind speed

For all nine datasets, upward sensible heat flux was observed with a weakly stable air–sea difference of potential temperature, and that upward flux became more prevalent with stronger winds. This systematic behavior occurs in all of the field programs in spite of their different measurement errors and processing. The countergradient flux is least frequent for weak winds. For wind speeds < 7 m s^{-1}, the heat flux statistically crosses zero for nonzero stable values of the air–sea temperature difference listed in the fifth column of Table 1.

This offset may be partly due to systematic measurement errors and could be influenced by postprocessing methods and radiometer calibration, which vary among field programs. For the weak-wind class, this offset is subtracted from the SST measurements in an attempt to normalize for temperature biases among the different field programs. Although this adjustment may remove true physical countergradient heat flux for weak winds, it allows examination of the wind speed dependence collectively for all of the datasets with less concern for variation of systematic errors for each field program. The qualitative behavior of the wind speed dependence found in this study is not affected by this adjustment of the SST.

3. Sensible heat flux

a. Dependence on $\theta_{sfc} - \theta(z)$

We now examine the relationship between the sensible heat flux and sea–air temperature difference, $\theta_{sfc} - \theta(z)$, for the GOTEX data for 10-km segments with no adjustment of the SST. Here, θ_{sfc} is the surface temperature and $\theta(z)$ is the potential temperature at flight level.

The sensible heat flux as a function of $\theta_{sfc} - \theta(z)$ tends not to intersect the origin but rather vanishes for negative (stable) values of $\theta_{sfc} - \theta(z)$ (Fig. 1). That is, for near-zero $\theta_{sfc} - \theta(z)$, most of the cases correspond to upward sensible heat flux. This offset in the GOTEX data is also evident in Fig. 5b of Raga and Abarca (2007), particularly after converting their air–sea temperature difference to a difference in potential temperature. Stable stratification with upward sensible heat flux (top-left quadrant of Fig. 1) is more common than unstable stratification with downward sensible heat flux (bottom-right quadrant of Fig. 1), which contains only one case from the strong-wind category. The magnitude of the offset of $\theta_{sfc} - \theta(z)$ increases with increasing wind speed (Fig. 1).

The subjectively determined offset is relatively small for wind speeds less than 14 m s^{-1} (green) but increases to about -0.3 K, on average, for winds between 14 and 20 m s^{-1} (black) and increases to more than -1 K for winds greater than 20 m s^{-1} (red). The influence of wind speed on the heat flux extends across the entire range of $\theta_{sfc} - \theta(z)$ (Fig. 1) but leads to countergradient fluxes mainly for small negative (stable) values of $\theta_{sfc} - \theta(z)$. The countergradient upward heat flux reaches values on the order of 0.01 K m s^{-1} ($\approx$10 W m^{-2}), which over large areas can be climatologically significant.

The offset in the relationship between the sensible heat flux and the air–sea temperature difference could be due to a number of physical causes in addition to any measurement errors that might be wind speed dependent. Some examples follow:

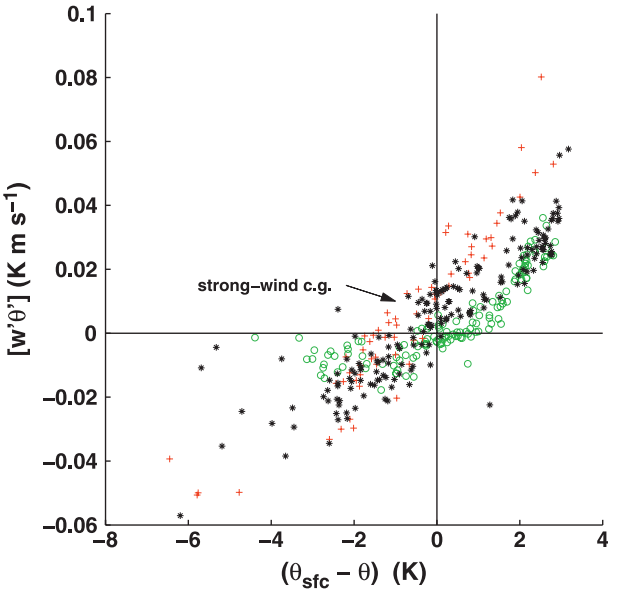

FIG. 1. Sensible heat flux as a function of $\theta_{sfc} - \theta(z)$ in GOTEX for different wind speed intervals (τ = 1 km, τ_F = 10 km): 0–14 m s^{-1} (green circles), 14–20 m s^{-1} (black asterisks), and >20 m s^{-1} (red pluses).

1) Sea spray can lead to countergradient transfer of sensible heat for strong winds (section 1 and Fig. 2, top middle), at least when the air temperature is measured above the spray layer (Andreas 2011).
2) Microscale wave breaking at moderate wind speeds can disrupt the cool skin layer and produce brief micropatches of relatively warm surface water (Zappa et al. 2004), as sketched in Fig. 2 (top left). Such a mechanism could lead to upward area-averaged sensible heat flux without reversing the weak stable stratification.
3) Patches of foam are observed to be cooler than the surrounding water surface (Marmorino and Smith 2005) and thus lower the area-averaged surface temperature (Fig. 2, top right) while not reversing the upward sensible heat flux. Bubbles in the foam may radiatively cool rapidly because of miniscule skin mass (K. Katsaros 2011, personal communication). Positive averaged air–sea temperature difference in the foam case (Fig. 2) requires that the averaged magnitude of the positive air–sea temperature difference is significantly greater than the averaged magnitude of the negative air–sea temperature difference. Although this distribution is observed for mesoscale variations of the sea surface temperature, adequate observations are unavailable on the wave scale.
4) Interpreting infrared measurements is complicated by the variation of emissivity and reflectivity with wavelength, the roughness of the sea surface, and the exact penetration depth of the infrared radiation

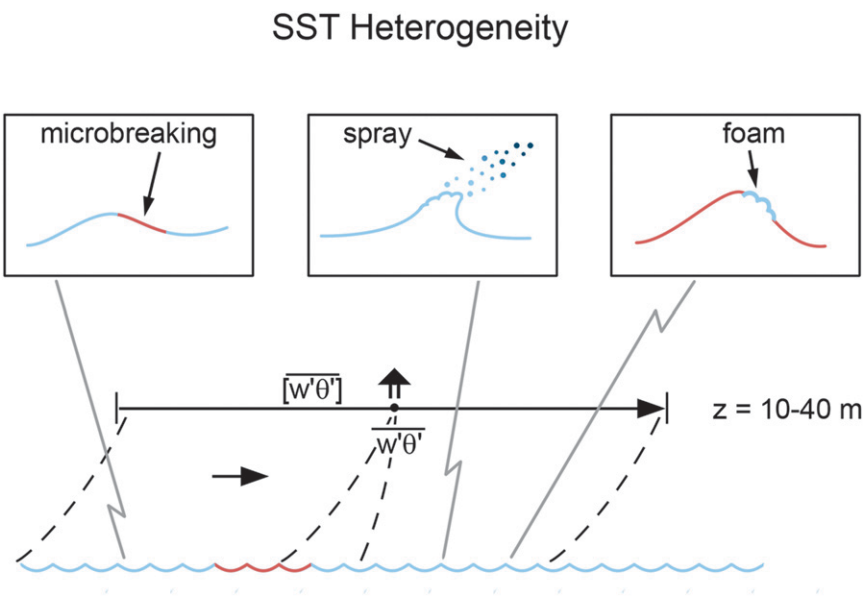

FIG. 2. Plausible scenarios for microscale heterogeneity for (top right) foam, (top middle) spray, and (top left) disruption of the cool skin layer by wave breaking and (bottom) mesoscale heterogeneity of the SST. Red surfaces identify SSTs that are greater than the air temperature, whereas blue surfaces identify SSTs that are less than the air temperature. The horizontal arrow in (bottom) depicts the aircraft flight leg, whereas the vertical dashed lines in the middle of the sketch denote the footprint of the upward sensible heat flux measured at a point along the aircraft track ($\overline{w'\theta'}$), symbolized by the upward double arrow. The vertical dashed lines near the edge of the track collectively define the surface footprint of the leg-averaged flux [$\overline{w'\theta'}$], whereas the vertical dashed lines near the center indicate the surface footprint for $\overline{w'\theta'}$. This sketch does not account for the crosswind influence on the footprint of the flux measured by the aircraft. The bottom panel depicts the potential countergradient flux of sensible heat on the mesoscale as discussed in the introduction.

through strong vertical gradients of temperature in the oceanic skin layer (Katsaros 1980; Donlon et al. 2002). Foam can reduce the emissivity, which reduces the emitted longwave radiation. This reduction leads to underestimation of the SST and possible false evidence of countergradient sensible heat flux. However, in cases of large downward longwave radiation, the reflected longwave radiation may be larger and lead to an overestimation of the SST. After considering a variety of additional errors, Burns et al. (2000) find that, in the balance, aircraft measurements overestimate the SST. This bias would produce an opposite result compared to our findings.

5) Greater aircraft roll angles with stronger turbulence cause more atmospheric contamination through increased pathlength between the aircraft radiometer and the sea surface, although this error is thought to be small.
6) Aircraft data collected over regions of mixed upward and downward sensible heat flux could underestimate the downward sensible heat flux in stable areas because of thin boundary layers and flux divergence between the surface and the aircraft level (Mahrt et al. 1998, 2001; Fairall et al. 2006; Vickers and Mahrt 2006; Kalogiros and Wang 2011), although it is not obvious how this effect increases the offset with strong winds.
7) For strong winds perpendicular to the flight track, the footprint of the measured flux at the aircraft level can be displaced from the measurement of the underlying sea surface temperature. It is not obvious how this influence would lead to systematic upward sensible heat flux for slightly stable conditions.
8) The influence of errors in the measured SST due to reflected downward longwave radiation could be correlated with wind speed if cloud cover decreased with increasing wind speed. We did not generally observe this relationship for our datasets.

Although aircraft data can assess the influence of mesoscale surface heterogeneity, subject to possible large flux sampling errors, aircraft data can only indirectly infer the possible influence of microscale SST heterogeneity. As an instructive exercise, we adjust the sea surface temperature to reduce the number of countergradient sensible heat flux cases. For example, the simple formulation

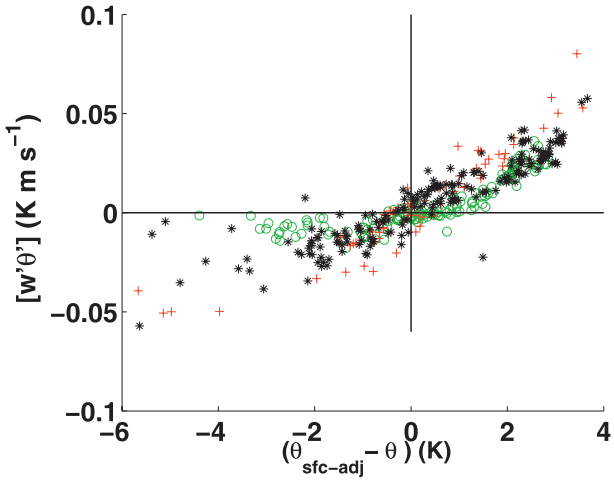

FIG. 3. Sensible heat flux in GOTEX as a function of $\theta_{sfc} - \theta(z)$ based on the adjusted surface temperature [Eq. (4)] for $\tau = 1$ km and $\tau_F = 10$ km, for wind speeds of 0–14 m s^{-1} (green circles), 14–20 m s^{-1} (black asterisks), and >20 m s^{-1} (red pluses).

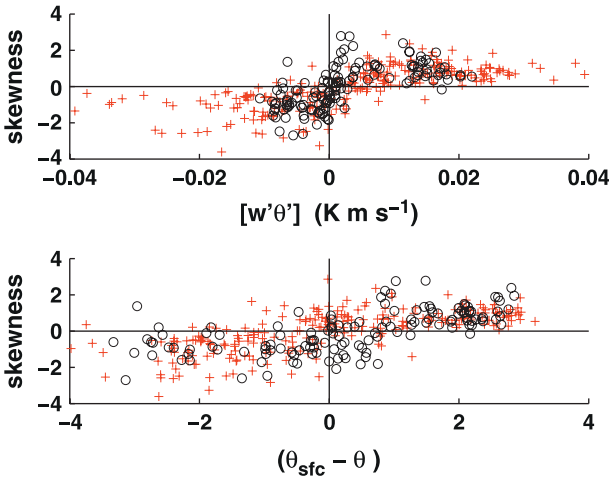

FIG. 4. (top) Skewness of the 200-m heat flux within 10-km windows as a function of the averaged heat flux for wind speeds less than 14 m s^{-1} (black circles) and for wind speeds greater than 14 m s^{-1} (red pluses). (bottom) Skewness of the 200-m heat flux within 10-km windows as a function of the averaged air–sea temperature difference for wind speeds less than 14 m s^{-1} (black circles) and for wind speeds greater than 14 m s^{-1} (red pluses).

$$\theta_{\text{sfc-adj}} = \theta_{\text{sfc}} + 0.1\,\text{K s m}^{-1}(V - 14\,\text{m s}^{-1}) \qquad (4)$$

significantly reduces the number of countergradient cases as is evident by comparing Fig. 3 with Fig. 1. Here, V is the flight-level wind speed, θ_{sfc} is the measured surface potential temperature, and $\theta_{sfc\text{-}adj}$ is the adjusted surface potential temperature that reduces the number of countergradient cases.

This adjustment of surface temperature decreases the differences among wind speed classes for the near-neutral range of the air–sea temperature difference (Fig. 3). Because the measured θ_{sfc} may include calibration errors, our interest is in the variation of the temperature offset with wind speed, not the averaged magnitude of the adjustment. The choice of 14 m s^{-1} is arbitrary because the impact of wind speed begins gradually with increasing wind speed.

As an aside, we have alternatively plotted $[w'\theta']/V$ versus $\theta_{sfc} - \theta(z)$ (not shown), which is dimensionally more consistent and more relevant to the bulk formula. However, such an analysis weights weak-wind cases, whereas the current study requires emphasis on stronger wind cases and also requires dimensional analysis of the heat flux without scaling.

b. Turbulence characteristics

The turbulence in the strong-wind, weakly stratified regime with upward heat flux is generated primarily by shear. The shear generation term in the turbulent kinetic energy equation is roughly two orders of magnitude larger than the buoyancy production term, even after allowing for potential significant errors in the shear estimate and including the contribution of the moisture flux to the buoyancy flux. Thus, the turbulence is produced primarily by shear generation. The skewness of the perturbations of potential temperature and vertical velocity are small in contrast to values in the convective regime, where the buoyancy generation of turbulence is dominant. Inspection of the time series of fast response variables do not reveal sharp cliff–ramp structures of a preferred sign in contrast to more convective conditions (e.g., Wilczak 1984; Mahrt 1991).

The skewness of the 200-m heat flux ($\tau = 200$ m) within a 10-km window ($\tau_F = 10$ km) is generally determined by the sign of the heat flux (Fig. 4, top), as expected from previous studies. In particular, the strong-wind slightly stable regime with upward heat flux (countergradient) shows generally positive skewness of the heat flux (top-left quadrant of Fig. 4, bottom). For weakly unstable conditions and weaker winds, the skewness of the heat flux is mostly negative, opposite of the expected value for positive heat flux. More detailed behavior of the turbulence in this regime and the countergradient regime will be reported in a future study.

c. Scale dependence τ

We now examine whether the above results are significantly influenced by the choice of averaging scales (defined in section 3a). Averaging the fluxes over $\tau_F = 40$ km instead of 10 km should reduce the random flux error by a factor of 2; however, a reduction of scatter in the relationship between the heat flux and the air–sea

temperature difference is not evident for these data (not shown). This result could imply that increasing τ_F captures more surface heterogeneity and contributes to the scatter. The temperature offset for $\tau_F = 40$ km is about twice as large as that for 10 km (not shown). The increased magnitude of the offset of $\theta_{\rm sfc} - \theta(z)$ for larger τ_F is consistent with capturing increased sea surface heterogeneity. Nine flights are not sufficient to isolate the dependence of random errors and surface heterogeneity on the flux-averaging length τ_F. However, our inspection of individual flight records reveals that SST heterogeneity probably explains some of the temperature offset. Although the impact of surface heterogeneity is normally thought to decrease with increasing wind speed, the strong winds of narrow horizontal extent in GOTEX induce increased mixing in the ocean surface layer and a band of cooler SST.

Figure 5 reveals the sensible heat flux as a function of intervals of $\theta_{\rm sfc} - \theta(z)$ equal to 1 K for three different ranges of horizontal scale. The 0–200-m flux is computed using $\tau = 200$ m. The 200–1000-m flux is computed by subtracting the 0–200-m flux from the 1-km flux ($\tau = 1$ km). The 1–5-km flux is computed by subtracting the 1-km flux from the 5-km flux ($\tau = 5$ km). The fluxes for the three scale ranges sum to the 5-km flux ($\tau = 5$ km) because all averages are unweighted and 200 m, 1 km, and 5 km are integer multiples.

The 0–200-m flux (Fig. 5, black) dominates the total flux for all wind speeds and $\theta_{\rm sfc} - \theta(z)$ categories. The standard error divided by the magnitude of the interval-averaged sensible heat flux is small compared to unity except where the sensible heat flux is particularly small. For this crude resolution for $\theta_{\rm sfc} - \theta(z)$, the significance of the 0–200-m countergradient sensible heat flux and its increase with wind speed is supported mainly by the interpolation from adjacent intervals of $\theta_{\rm sfc} - \theta(z)$. This behavior is also supported by consulting Fig. 1, where the strong-wind cases for weak stability -1.0 K $< \theta_{\rm sfc} - \theta(z) < 0$ K all correspond to upward sensible heat flux. Averaging over smaller intervals of $\theta_{\rm sfc} - \theta(z)$ (not shown) generally leads to more significant sampling problems.

The sensible heat flux for the 200–1000-m range of scales is of marginal importance, except for the most unstable conditions (right-hand side of Fig. 5), where it can account for about one-third of the flux. The importance of the larger-scale flux for a given interval of $\theta_{\rm sfc} - \theta(z)$ increases with increasing wind component along the flight track (not shown). Elongation of the eddies in the flight direction shifts the transport to larger scales (Lenschow 1970).

The sensible heat flux for the range of scales between 1 and 5 km is generally unimportant, at least in terms of interval averages. This 1–5-km sensible heat flux is important for individual sublegs but does not have a preferred sign such that averaging over sublegs reduces its importance through cancellation. These results are similar to the findings of Sun et al. (1996). The ability of the aircraft to measure fluxes on such large scales is uncertain, although the analysis of Lenschow and Sun (2007) suggests that sufficiently accurate flux estimates are plausible.

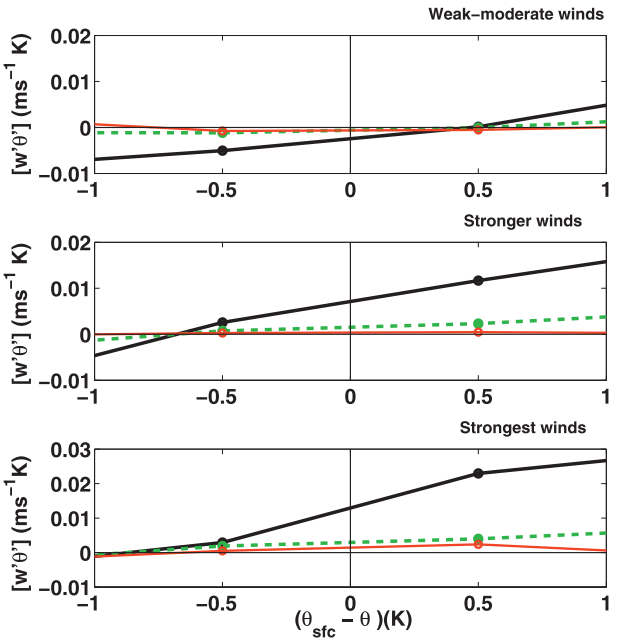

FIG. 5. Subleg sensible heat flux in GOTEX for three different scale ranges: 0–200 m (black), 200–1000 m (green), and 1–5 km (red). Here, $\tau_F = 10$ km. Sensible heat fluxes are averaged over different intervals of $\theta_{\rm sfc} - \theta(z)$. Wind speed classes are (top) 0–14 m s^{-1}, (middle) 14–20 m s^{-1}, and (bottom) >20 m s^{-1}.

4. Additional datasets

We now analyze the sensible heat flux based on 4-km records aggregated from all nine field programs (section 2 and Table 1). This much larger sample size from the combined dataset allows us to construct four wind speed classes instead of three classes: here, <7 m s^{-1}, 7–14 m s^{-1}, 14–21 m s^{-1}, and >21 m s^{-1}. To reduce the impact of large random flux errors, we composite the sensible heat flux over all of the field programs for different intervals of $\theta_{\rm sfc} - \theta(z)$ for each wind speed class. The corresponding composited sensible heat flux is upward for small negative (stable) values of $\theta_{\rm sfc} - \theta(z)$ (Fig. 6) for the three stronger wind classes.

Figure 6 shows the composited sensible heat flux crosses zero for stable conditions corresponding to approximately $\theta_{\rm sfc} - \theta(z) = -0.35$ K for the wind speed class of 7–14 m s^{-1} (black), -0.6 K for the wind

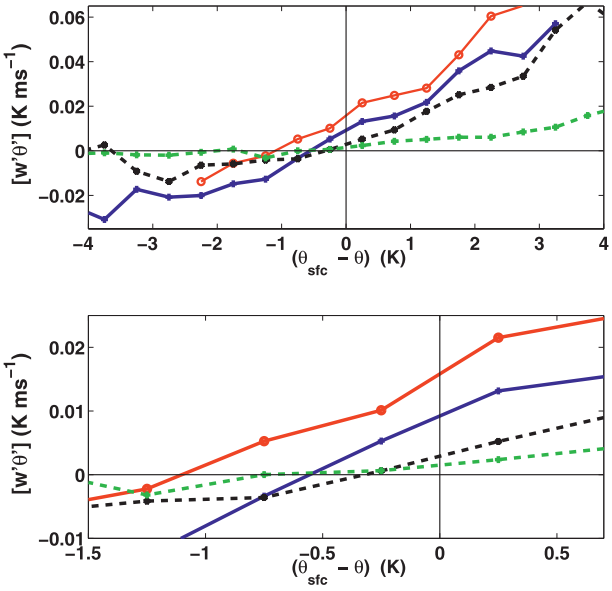

FIG. 6. (top) The sensible heat flux composited over intervals of $\theta_{sfc} - \theta(z)$ using the 4-km values ($\tau = \tau_F = 4$ km) collectively for all nine field programs for wind speeds of <7 m s^{-1} (green dashed), 7–14 m s^{-1} (black dashed), 14–21 m s^{-1} (blue solid), and >21 m s^{-1} (red solid). (bottom) For near-neutral conditions.

speed class of 14–21 m s^{-1} (blue), and −1.2 K for the wind speed class of >21 m s^{-1} (red). The cause of the closeness of the crossover values of $\theta_{sfc} - \theta(z)$ for the 7–14 m s^{-1} and 14–21 m s^{-1} wind speed classes (Fig. 6) is not known. However, different field programs contribute differently to different wind speed classes such that the increase of the negative crossover value of $\theta_{sfc} - \theta(z)$ with increasing wind speed can be interpreted only qualitatively.

The standard error for the interval-averaged sensible heat flux is small compared to the interval-averaged value for most of the $\theta_{sfc} - \theta(z)$ intervals for the different wind speed classes, except when the interval-averaged value of the sensible heat flux is very small. Although the scatter is large within individual intervals, the standard error is generally small compared to the absolute value of the sensible heat flux because the dataset is very large (Table 1).

5. Conclusions

This study examined the relationship of the sea surface sensible heat flux to the wind speed and air–sea temperature difference using the GOTEX aircraft data, supplemented by eight other aircraft datasets. This analysis emphasized common near-neutral conditions, usually neglected in previous studies because of uncertainties in the air–sea temperature difference.

For slightly stable stratification (sea surface cooler than the air), the sensible heat flux is, on average, upward ("countergradient"). This countergradient contribution increases with increasing wind speed. In addition to unknown measurement errors, potential causes of this countergradient sensible heat flux include microscale variations of surface temperature induced by wave breaking and foam, heat fluxes mediated by sea spray, and mesoscale variation of sea surface temperature within the averaging area. Our analysis shows that surface heterogeneity sometimes contributes significantly to the countergradient flux but is not an overall explanation. Instrumentation errors that cause underestimation of the SST, which increase with increasing wind speed, have not been identified, but this possibility requires more investigation.

The current strategy for field programs is not adequate for rigorously resolving the various issues raised in this study. Measurements substantially closer to the surface compared to the usual 30–40-m flight levels would improve the estimates of the surface fluxes. More accurate SST measurements, with SST errors on the order of 0.1 K or less, would be beneficial. Such measurements would require continual calibration and documentation during the field program as well as accurate estimates of the reflected downward longwave radiation. Finally, analysis of the dependence of fluxes on averaging scale is essential for near-neutral conditions, where the turbulence may vary between slightly stable and slightly unstable conditions along the flight track.

Acknowledgments. Helpful comments from Chris Fairall and the reviewers and discussions with Kristina Katsaros and Andy Jessup are greatly appreciated. The U.S. Office of Naval Research supported Mahrt, Vickers, and Andreas in this work through Award N00014-11-1-0073. Mahrt was additionally supported by ONR Grant N00014-11-WX20724. Khelif is supported by ONR Grant N00014-08-1-0438.

REFERENCES

Anderson, K., and Coauthors, 2004: The RED experiment: An assessment of boundary layer effects in a trade winds regime on microwave and infrared propagation over the sea. *Bull. Amer. Meteor. Soc.,* **85,** 1355–1365.

Andreas, E. L, 1995: The temperature of evaporating sea spray droplets. *J. Atmos. Sci.,* **52,** 852–862.

——, 2011: Fallacies of the enthalpy transfer coefficient over the ocean in high winds. *J. Atmos. Sci.,* **68,** 1435–1445.

——, and K. A. Emanuel, 2001: Effects of sea spray on tropical cyclone intensity. *J. Atmos. Sci.,* **58,** 3741–3751.

Burns, S. P., and Coauthors, 2000: Comparisons of aircraft, ship, and buoy radiation and SST measurements from TOGA COARE. *J. Geophys. Res.,* **105,** 15 627–15 652.

Donlon, C. J., P. J. Minnett, C. Gentemann, T. Nightingale, J. Barton, B. Ward, and M. J. Murray, 2002: Toward improved validation of satellite sea surface skin temperature measurements for climatic research. *J. Climate,* **15,** 353–369.

Edson, J. B., and Coauthors, 2007: The Coupled Boundary Layers and Air–Sea Transfer experiment in low winds. *Bull. Amer. Meteor. Soc.,* **88,** 341–356.

Fairall, C. W., and Coauthors, 2006: Turbulent bulk transfer coefficients and ozone deposition velocity in the International Consortium for Atmospheric Research into Transport and Transformation. *J. Geophys. Res.,* **111,** D23S20, doi:10.1029/2006JD007597.

Grachev, A., C. Fairall, J. Hare, J. Edson, and S. Miller, 2003: Wind stress vector over ocean waves. *J. Phys. Oceanogr.,* **33,** 2408–2429.

Hagan, D., D. Rogers, C. Friehe, R. Weller, and E. Walsh, 1997: Aircraft observations of sea surface temperature variability in the tropical Pacific. *J. Geophys. Res.,* **102,** 15 733–15 747.

Kalogiros, J., and Q. Wang, 2011: Aircraft observations of sea-surface turbulent fluxes near the California coast. *Bound.-Layer Meteor.,* **139,** 283–306.

Katsaros, K., 1980: Radiative sensing of sea surface temperature. *Air-Sea Interaction: Instruments and Methods,* F. Dobson, L. Hasse, and R. Davis, Eds., Plenum Press, 293–317

——, and A. V. Soloviev, 2004: Vanishing horizontal sea surface temperature gradients at low wind speeds. *Bound.-Layer Meteor.,* **112,** 381–396.

——, ——, R. H. Weisberg, and M. E. Luther, 2005: Reduced horizontal sea surface temperature gradients under conditions of clear skies and weak winds. *Bound.-Layer Meteor.,* **116,** 175–185.

Lenschow, D. H., 1970: Airplane measurements of planetary boundary layer structure. *J. Appl. Meteor.,* **9,** 874–884.

——, and J. Sun, 2007: The spectral composition of fluxes and variances over land and sea out to the mesoscale. *Bound.-Layer Meteor.,* **125,** 63–84.

Mahrt, L., 1991: Eddy asymmetry in the sheared heated boundary layer. *J. Atmos. Sci.,* **48,** 472–492.

——, and D. Khelif, 2010: Heat fluxes over weak SST heterogeneity. *J. Geophys. Res.,* **115,** D11103, doi:10.1029/2009JD013161.

——, D. Vickers, J. Edson, J. Sun, J. Højstrup, J. Hare, and J. M. Wilczak, 1998: Heat flux in the coastal zone. *Bound.-Layer Meteor.,* **86,** 421–446.

——, ——, J. Sun, T. L. Crawford, G. Crescenti, and P. Frederickson, 2001: Surface stress in offshore flow and quasi-frictional decoupling. *J. Geophys. Res.,* **106,** 20 629–20 639.

Marmorino, G. O., and G. B. Smith, 2005: Bright and dark ocean whitecaps observed in the infrared. *Geophys. Res. Lett.,* **32,** L11604, doi:10.1029/2005GL023176.

——, ——, and G. J. Lindemann, 2004: Infrared imagery of ocean internal waves. *Geophys. Res. Lett.,* **31,** L11309, doi:10.1029/2004GL020152.

Raga, G. B., and S. Abarca, 2007: On the parameterization of turbulent fluxes over the tropical eastern Pacific. *Atmos. Chem. Phys.,* **7,** 635–643.

Smedman, A.-S., U. Högström, J. Hunt, and E. Sahlée, 2007a: Heat/mass transfer in the slightly unstable atmospheric surface layer. *Quart. J. Roy. Meteor. Soc.,* **133,** 37–51.

——, ——, E. Sahlée, and C. Johansson, 2007b: Critical re-evaluation of the bulk transfer coefficient for sensible heat over the ocean during unstable and neutral conditions. *Quart. J. Roy. Meteor. Soc.,* **133,** 227–250.

Soloviev, A., and R. Lukas, 2006: *The Near-Surface Layer of the Ocean: Structure, Dynamics and Applications*. Springer, 572 pp.

Sun, J., J. F. Howell, S. K. Esbensen, L. Mahrt, C. M. Greb, R. Grossman, and M. A. LeMone, 1996: Scale dependence of air–sea fluxes over the western equatorial Pacific. *J. Atmos. Sci.,* **53,** 2997–3012.

——, D. Vandemark, L. Mahrt, D. Vickers, T. Crawford, and C. Vogel, 2001: Momentum transfer over the coastal zone. *J. Geophys. Res.,* **106,** 12 437–12 488.

Vickers, D., and L. Mahrt, 2006: Evaluation of the air-sea bulk formula and sea-surface temperature variability. *J. Geophys. Res.,* **111,** C05002, doi:10.1029/2005JC003323.

Walsh, E. J., 1998: Coupling of internal waves on the main thermocline to the diurnal surface layer and sea surface temperature during the Tropical Ocean-Global Atmosphere Coupled Ocean-Atmosphere Response Experiment. *J. Geophys. Res.,* **103,** 12 613–12 628.

Wilczak, J., 1984: Large-scale eddies in the unstably stratified atmospheric surface layer. Part I: Velocity and temperature structure. *J. Atmos. Sci.,* **41,** 3537–3550.

Zappa, C. J., W. E. Asher, A. T. Jessup, J. Klinke, and S. R. Long, 2004: Microbreaking and the enhancement of air-water transfer velocity. *J. Geophys. Res.,* **109,** C08S16, doi:10.1029/2003JC001897.

Zeng, X., M. Zhao, and R. E. Dickinson, 1998: Intercomparison of bulk aerodynamic algorithms for the computation of sea surface fluxes using TOGA COARE and TAO data. *J. Climate,* **11,** 2628–2644.